J. theor. Biol. (2000) **206,** 181–194
doi:10.1006/jtbi.2000.2113, available online at http://www.idealibrary.com on IDEAL®

A Computational Study of the Effect of Capillary Network Anastomoses and Tortuosity on Oxygen Transport

Daniel Goldman* and Aleksander S. Popel

Department of Biomedical Engineering and Center for Computational Medicine and Biology, Johns Hopkins University School of Medicine, Baltimore, MD 21205, *U.S.A.*

(*Received on* 20 *October* 1999, *Accepted in revised form on* 22 *May* 2000)

The objective of this study was to investigate the effects of capillary network anastomoses and tortuosity on oxygen transport in skeletal muscle, as well as the importance of muscle fibers in determining the arrangement of parallel capillaries. Countercurrent flow and random capillary blockage (e.g. by white blood cells) were also studied. A general computational model was constructed to simulate oxygen transport from a network of blood vessels within a rectangular volume of tissue. A geometric model of the capillary network structure, based on hexagonally packed muscle fibers, was constructed to produce networks of straight unbranched capillaries, capillaries with anastomoses, and capillaries with tortuosity, in order to examine the effects of these geometric properties. Quantities examined included the tissue oxygen tension and the capillary oxyhemoglobin saturation. The computational model included a two-phase simulation of blood flow. Appropriate parameters were chosen for working hamster cheek-pouch retractor muscle. Our calculations showed that the muscle-fiber geometry was important in reducing oxygen transport heterogeneity, as was countercurrent flow. Tortuosity was found to increase tissue oxygenation, especially when combined with anastomoses. In the absence of tortuosity, anastomoses had little effect on oxygen transport under normal conditions, but significantly improved transport when vessel blockages were present.

Introduction

Oxygen is one of the most important substances that the circulation must deliver to living cells. In skeletal muscle, demand for oxygen can increase more than ten-fold during exercise, making oxygen delivery particularly critical. Although oxygen transport from arterioles and venules is more significant than once thought (Ellsworth *et al.*, 1994), capillaries are a major site of oxygen delivery. Many theoretical studies have been performed of oxygen transport from capillaries in skeletal muscle, starting with the work of August Krogh (1919). The simple Krogh model of uniformly spaced and supplied parallel capillaries leads to exact mathematical results that are valuable in the understanding of oxygen transport. However, the geometry and hemodynamics of capillary networks in skeletal muscle are actually much more complicated than Krogh assumed (Ellsworth *et al.*, 1994; Pittman, 1995). The capillaries that run parallel to muscle fibers are not perfectly straight or uniformly spaced, and there

* Author to whom correspondence should be addressed. E-mail: dgoldman@bme.jhu.edu

0022–5193/00/180181 + 14 $35.00/0

are cross-connections or anastomoses between them. This geometric complexity is compounded by differences in blood supply amongst the parallel vessels. Some of these flow differences are due to the capillary network structure itself, while others are due to differences at the level of feeding arterioles or draining venules. In addition, microcirculatory oxygen transport is complicated by the fact that oxygen can diffuse directly into or out of both arterioles and venules. Thus, in reality oxygen is supplied in a way that is spatially complex and can lead to significant heterogeneity in the amount of oxygen available to individual parenchymal cells. Oxygen delivery has similar spatial complexity in other tissues, such as heart and brain; striated muscle is studied as an important first step.

Under resting conditions, most tissue regions are convectively well supplied with oxygen, and differences in oxyhemoglobin saturation (SO_2) between nearby capillaries are smoothed out by diffusion (Ellsworth *et al*., 1988). During exercise, oxygen delivery heterogeneities may not be compensated for by diffusion, resulting in a higher degree of heterogeneity of steady-state oxygen tension in the tissue (Klitzman *et al*., 1983; Ellsworth *et al*., 1988). This heterogeneity, which can include regions of potentially damaging hypoxia, and its relationship with structural properties of the microcirculation are poorly understood at the present time. The goal of the work presented here is to investigate the role of capillary network complexity in producing heterogeneity in the spatial distribution of tissue oxygen tension (PO_2), and for this purpose working striated muscle is the primary focus. Capillary networks in striated muscle are known to be organized into modules (Berg & Sarelius, 1995). In the present work we concentrate on small numbers of capillaries, which can be considered to represent functional modules.

Previous computational models investigated aspects of oxygen transport heterogeneity in skeletal muscle (Popel *et al*., 1986; Ellsworth *et al*., 1988; Groebe, 1990; Secomb & Hsu, 1994; Hoofd & Turek, 1996). Following this work, we have constructed a biophysically detailed model to study the effect of microvascular network complexity on tissue oxygen delivery. In the present study we focus on anastomoses between "parallel" capillaries and capillary tortuosity, as well as the arrangement of the parallel capillaries. The model presented is sufficiently general to allow the systematic investigation of various other aspects of vascular and cellular heterogeneity in the future, in muscle and other tissues. In particular, it will enable us to utilize the detailed structural, hemodynamic, and oxygenation data that emerging techniques of 3D space–time video-image analysis of the microvasculature will provide (Ellis *et al*., 1992; Japee, 1999).

Mathematical Model

BLOOD FLOW AND OXYGEN TRANSPORT

A computational model was used to calculate blood flow and oxygen transport in the capillary network/tissue geometries studied. A two-phase continuum flow model was used to calculate the distribution of total blood flow (Q) and discharge (flow-averaged) hematocrit (H_D) throughout each capillary network. The flow model was based on the *in vivo* rheological model of Pries *et al*. (1994) and involves the following conservation equations for blood and erythrocyte volume flow into each node j:

$$\sum_i Q_{ij} = 0, \tag{1}$$

$$\sum_i H_{Dij} Q_{ij} = 0, \tag{2}$$

where each vessel segment ij is labeled by its end nodes and the sums are over all nodes i connected to node j. Since bifurcations are the only type of vessel branching considered, each node is connected to at most three other nodes. The flow in segment ij is given by the pressure difference across the segment divided by the hydrodynamic resistance of the segment, $Q_{ij} = (p_i - p_j)/r_{ij}$. Blood vessels are assumed to have circular cross-sections, and since both Reynolds and Womersley numbers are very low in the microcirculation, flow resistance can be expressed in the form of Poiseuille's Law

$$r_{ij} = \frac{8\eta L}{\pi R^4}, \tag{3}$$

where L and R are the length and radius of the vessel segment being considered and η is the apparent viscosity of blood, which is known to vary with hematocrit and vessel diameter (the Fahraeus–Lindqvist effect).

Pries *et al.* (1994) have obtained an empirical expression for the apparent viscosity of blood *in vivo*, $\eta = f_1(D, H_D)$ where D is the vessel diameter, based on experiments in rat mesentery. Since equations were presented in terms of human blood parameters, for the current study values of D were rescaled using the hamster and human erythrocyte volumes, approximately 69.3 and 92 fl, respectively. Thus, $D = (V_{human}/V_{hamster})^{1/3} D_{hamster}$, where $D_{hamster}$ is the vessel diameter in the present simulations.

The Fahraeus–Lindqvist effect is one result of the fact that blood is a complex fluid. Another is the phenomenon known as plasma skimming, where erythrocyte flow at vessel bifurcations is distributed more unevenly than overall blood flow. To describe this effect, we used the expression of Pries *et al.* (1990) at diverging bifurcations, in addition to erythrocyte volume flow conservation: $H_1 = H_0 f_2(Q_1/Q_0, D_0, D_1, D_2)$, where H_0 and Q_0 are the hematocrit and flow in the parent vessel, H_1 and Q_1 are the hematocrit and flow in the first of the two daughter vessels, and D_0, D_1, D_2 are the diameters of the parent vessel and the first and second daughter vessels.

The required boundary conditions for the flow calculations are the pressure at all exterior nodes and the discharge hematocrit in all inflow segments. Solutions are obtained iteratively, due to the nonlinearity introduced by the Fahraeus–Lindqvist and plasma-skimming effects.

The oxygen transport model used was similar to that described by Popel (1989), but also included myoglobin-facilitated diffusion in the tissue and dissolved oxygen in the blood. The muscle tissue was taken to be continuous with constant material properties, while blood was taken to be a mixture of erythrocytes and plasma. Intracapillary transport resistance, as well as that due to the capillary wall and interstitium, was included using mass transfer coefficients. Transport in the tissue was described by the following equation for the steady-state oxygen tension, $P(x, y, z)$:

$$D\nabla^2 P + \frac{1}{\alpha} D_{Mb} c_{Mb} \nabla \cdot \left(\frac{\mathrm{d}S_{Mb}}{\mathrm{d}P} \nabla P \right) - \frac{1}{\alpha} M(P) = 0, \tag{4}$$

where α and D are the tissue oxygen solubility and diffusivity, respectively, $M(P)$ is the oxygen consumption, and c_{Mb}, D_{Mb}, and S_{Mb} are the myoglobin (Mb) concentration, diffusivity, and oxygen saturation.

Oxygen transport in the blood vessels was described by a steady-state equation for the capillary SO_2, $S(\xi)$:

$$v_b \frac{\partial S}{\partial \xi} + \frac{1}{\pi R} \left[H_D C_{Hb} + \alpha_b \frac{\mathrm{d}P_b}{\mathrm{d}S} \right]^{-1} \oint j \, \mathrm{d}\theta = 0, \tag{5}$$

where v_b is the mean blood velocity, ξ is the curvilinear coordinate along the axis of a given capillary, θ is the circumferential coordinate about the local capillary axis, R is the capillary radius, and P_b is the blood oxygen tension. Equation (5) is derived from a pair of equations for plasma and erythrocyte oxygen content by assuming that plasma PO_2 is equal to intraerythrocyte PO_2 (see the appendix). In general, plasma PO_2 is lower; however, this assumption introduces only a very small error and allows plasma-dissolved oxygen to be considered, which was not the case in previous models (e.g. Ellsworth *et al.*, 1988; Secomb & Hsu, 1994).

The blood oxygen solubility, which describes dissolved oxygen in both the erythrocytes and plasma, is given by (Klitzman *et al.*, 1983)

$$\alpha_b = H_D \alpha_{cell} + (1 - H_D) \alpha_{pl}, \tag{6}$$

where α_{cell} and α_{pl} are the oxygen solubilities inside the erythrocyte and in the plasma. The oxygen binding capacity of blood is $H_D C_{Hb}$, where C_{Hb} is the binding capacity of hemoglobin. The oxygen flux at a point (ξ, θ) on the capillary/tissue interface is

$$j = k(P_b - P_w), \tag{7}$$

TABLE 1
Biophysical parameters used in oxygen transport model. See text for descriptions

Parameter	Value	Units	References
α	3.89×10^{-5}	ml O_2 ml^{-1} mmHg^{-1}	Mahler *et al.* (1985)
D	2.41×10^{-5}	cm^2 s^{-1}	Bentley *et al.* (1993)
M_0	1.57×10^{-4}	ml O_2 ml^{-1} s^{-1}	Sullivan & Pittman (1984)
P_c	0.5	mmHg	Honig & Gayeski (1982)
c_{Mb}	1.02×10^{-2}	ml Mb ml^{-1}	Meng *et al.* (1993)
D_{Mb}	1.73×10^{-7}	cm^2 s^{-1}	Jurgens *et al.* (1994)
α_{pl}	2.82×10^{-5}	ml O_2 ml^{-1} mmHg^{-1}	Christoforides *et al.* (1969)
α_{cell}	3.38×10^{-5}	ml O_2 ml^{-1} mmHg^{-1}	Altman & Dittmer (1971)
P_{50}	29.3	mmHg	Ellsworth *et al.* (1988)
n	2.2	—	Ellsworth *et al.* (1988)
C_{Hb}	0.52	ml O_2 ml^{-1}	Clark *et al.* (1985)
$P_{50,Mb}$	5.3	mmHg	Jurgens *et al.* (1994)

where P_w is the tissue PO_2 at the capillary surface and k is the mass transfer coefficient.

The blood flow calculations give v_b and H_D in each capillary segment, and the boundary condition for eqn (5) is given by specifying S in each inlet segment. The boundary condition on P at the capillary surface is

$$-D\alpha \frac{\partial P_w}{\partial n} = j \tag{8}$$

and no-flux boundary conditions are specified at the outer tissue surfaces. In all calculations Michaelis–Menten consumption kinetics was assumed, $M(P) = M_0 P/(P + P_c)$, and the Hill equation was used for the oxyhemoglobin saturation curve, $S(P) = P^n/(P^n + P_{50}^n)$. Myoglobin oxygen saturation was given by $S(P) = P/(P + P_{50,Mb})$.

The biophysical parameters used in transport calculations, shown in Table 1, follow those of Ellsworth *et al.* (1988), except where more accurate values have become available (see Roy & Popel, 1996). The value used for myoglobin diffusivity is lower than the rotational value of Wang *et al.* (1997) but is consistent with the latest results of Papadopoulos *et al.* (2000) for translation in both radial and longitudinal fiber directions. Capillary wall mass transfer coefficients come from recently calculated, hematocrit-dependent values from this laboratory (A. R. Vadapalli, pers. comm.). Mass transfer coefficients were obtained as a function of the tube (volume-averaged) hematocrit, H_T, and the empirical formula of Pries *et al.* (1990), $H_T = f_3(D, H_D)$, was used to express k in terms of H_D for our flow calculations:

$$k(H_D) = (17.7H_D^2 - 1.07H_D + 0.672) \times 10^{-6} \text{ ml } O_2 \text{ s}^{-1} \text{ cm}^{-2} \text{ mmHg}^{-1}. \tag{9}$$

For $H_D = 0.47$ ($H_T = 0.43$) the above expression gives $k = 4.0 \times 10^{-6}$, in agreement with $k \approx 3.5 \times 10^{-6}$ obtained by converting the value of k from Eggleton *et al.* (1998), where k was normalized per unit capillary length. Mass transfer coefficients are known to be velocity-dependent (Groebe & Thews, 1989); however, Eggleton *et al.* showed that this dependence is weak in the working (high blood velocity) cases considered here.

NETWORK CONSTRUCTION AND FLOW CONDITIONS

The capillary network model used is based on the physiological structure of striated muscle and on measured geometric parameters, mainly those obtained for hamster cheek-pouch retractor muscle. Cylindrical muscle fibers of 40 μm diameter (Bennett *et al.*, 1991) and 400 μm length (Ellsworth *et al.*, 1988; Dong, 1997) are packed hexagonally, and straight parallel capillaries of 1.8 μm radius (Ellsworth *et al.*, 1988) are placed in the spaces between them (Fig. 1). After the construction of the capillary network, the width and

FIG. 1. Construction of capillary networks using hexagonally packed muscle fibers. After parallel vessels are placed between the fibers, anastomoses (shown) and tortuosity may be added.

height of the tissue cross-section are set to the minimum needed to enclose all geometrically related networks, and all points inside the three-dimensional domain but outside the capillaries are treated as muscle tissue. Muscle fiber boundaries are not considered in transport calculations in the present work. The network construction is random, but in keeping with a measured capillary density of approximately $1400/mm^2$ (Ellsworth *et al*., 1988; Dong, 1997), 11 parallel capillaries are used for the four muscle fibers considered. This network size is consistent with the average number of capillaries ($\sim$12) found experimentally by Berg & Sarelius (1995) for modules supplied by single arterioles. In addition, each network has, on average, 5.25 capillaries bordering each muscle fiber, based on measurements for the muscle modeled (Bennett *et al*., 1991). The networks just described, denoted as SU (straight unbranched), are considered the reference case. To investigate the effect of the muscle-fiber construction, we also placed parallel capillaries randomly in the tissue volume without regard for the muscle fibers. These networks are denoted as R (random).

To study the effect of anastomoses, cross-connections were added to the networks of parallel vessels produced with the muscle-fiber construction. Each of these networks, denoted as SA (straight anastomosed), had a specified number of anastomoses inserted between neighboring parallel vessels, with the cross-connections constrained to not intersect and have endpoints between 12.5 and 50 μm apart in the z-direction; the anastomoses were also constrained to wrap around the muscle fibers. The number of anastomoses was either equal to (SA_1 and SA_2) or twice (SA_3) the number of parallel capillaries, both of which add a physiologically reasonable amount of non-parallel capillary length or *tortuosity*, 9 and 18%, respectively (Mathieu-Costello, 1987).

To study the effect of tortuosity of the parallel vessels, sinusoidal variations (50 μm wavelength, 8 μm amplitude) were superimposed on the muscle-fiber-based networks. This added 19% tortuosity, which is approximately the amount observed in moderately contracted skeletal muscle (Mathieu-Costello *et al*., 1989). Networks with tortuosity were constructed both without anastomoses (TU, tortuous unbranched) and with anastomoses (TA, tortuous anastomosed).

In all the network types described above, the overall blood flow in each parallel capillary was in the positive z-direction (concurrent), due to a uniform pressure difference between the arterial and venous ends. To study the effect of countercurrent flow, the pressure gradient was reversed in two of the 11 parallel vessels in each of the SU networks, yielding networks denoted as SU-counter (straight unbranched countercurrent).

For each type of network geometry three realizations were studied. The discharge hematocrit and SO_2 were set to 0.43 and 0.63, respectively, at the inlets of all parallel vessels in all networks studied. The length of the tissue block was fixed at 400 μm, but to minimize edge effects the tissue cross-sectional area was adjusted depending on the realization (9803, 8003, or 9436 μm^2). Therefore, in order to maintain constant total blood flow per unit tissue volume, the flow through each network was rescaled in proportion to the tissue cross-section. In the networks with tortuosity (TU, TA), the increased vessel length resulted in increased hydrodynamic resistance and hence decreased blood flow. Therefore, the arterio-venous pressure difference was increased by approximately 18% in these networks to maintain constant blood flow. Since the nonlinearities in the flow model do not

depend on the magnitude of the blood velocity, adjusting the total flow (either directly or via the pressure gradient) does not change the flow distribution in the network.

METABOLIC STATE

Although working muscle was of primary interest, the arterio-venous pressure difference was set (at 10 mmHg) to match observed resting conditions, taken to be an average longitudinal velocity of approximately 100 $\mu m\, s^{-1}$ (Ellsworth *et al*., 1988; Dong, 1997). With the exception of one resting case (TA_1-rest), calculated flow rates were increased five-fold (to an average of 500 $\mu m\, s^{-1}$) and consumption was set at ten times resting ($10M_0 = 1.57 \times 10^{-3}$ ml O_2 $ml^{-1}\, s^{-1}$) in all oxygen transport calculations.

NUMERICAL METHOD

The transport equations were solved by adding time derivatives of P and S to the right-hand side of eqns (4) and (5), respectively, and advancing the solution until a steady state was reached. The tissue volume was discretized into a uniform rectangular grid and the capillaries were divided into short cylindrical segments. A finite-difference method was used with interpolation between the tissue grid and the capillary segments. A similar method was used in earlier studies (Popel *et al*., 1986; Ellsworth *et al*., 1988); however, in these cases all capillary segments were aligned with the z-axis and capillary bifurcations were not considered. In the present case, these restrictions were relaxed, making the geometric calculations much more complicated. In particular, in order to apply the boundary conditions for eqn (4) and calculate the wall flux for eqn (5), it was necessary to find the intersection of the tissue grid lines with the capillary cylinders and compute the normal vectors at each intersection point.

To solve the transport equations, an explicit time-stepping scheme was used, with central differencing for spatial derivatives and upwinding for the convective term in eqn (5). Before beginning the present study, the spatial accuracy of the numerical method was verified for several cases by refining the tissue and capillary discretizations. In addition, the simulation code was validated by comparing results directly to the Krogh–Erlang analytical solution for the case of a single straight capillary with constant O_2 consumption and no axial diffusion in the tissue. For the calculations discussed, the grid spacing in the tissue was approximately 1.5 μm in all directions and capillary segments were approximately 12.5 μm in length.

Blood Flow Heterogeneity

The objective of this study was to investigate the effect of the geometric complexity of microvascular networks on oxygen transport. One important aspect of this is the effect vessel bifurcations have on blood flow and hematocrit distributions in the network. As part of our oxygen transport simulations, Q and H_D were calculated in all the capillary networks studied, using the blood flow model. Examples of the geometries used can be seen in Fig. 2, which shows networks SA_1, SA_2, SA_3, and TA_3. In Table 2, we present results for the minimum, mean, and coefficient of variation (CV, S.D./mean) of Q and the erythrocyte volume flow $F = QH_D$ in the SU, SA, and TA network types. Here Q has *not* been adjusted for variations between realizations in tissue cross-sectional area. Only results for SU networks are shown because flow parameters are the same in all capillaries of all unbranched cases (SU, R, SU-counter, and TU). Figure 3 contains the normalized histograms of v_b obtained for the networks shown in Fig. 2. It can be seen that anastomoses change the uniform flow patterns in the unbranched networks into fairly wide flow distributions, qualitatively similar to those found experimentally (Klitzman & Johnson, 1982; Ellsworth *et al*., 1988).

Capillaries in the anastomosed cases have slightly lower mean Q (5.5 vs. 6.0 pl/s), H_D (0.42 vs. 0.43), and F (2.3 vs. 2.6 pl/s). However, the minimum values of F are significantly lower for the anastomosed cases (0.1 vs. 2.6 pl/s) and the coefficient of variation of F is $\sim 30\%$. Thus, capillary anastomoses were found to increase the spatial heterogeneity of erythrocyte supply, suggesting an increase in oxygen distribution heterogeneity. As will be discussed in the next section, the addition of anastomoses to networks without tortuosity (SA) increased transport

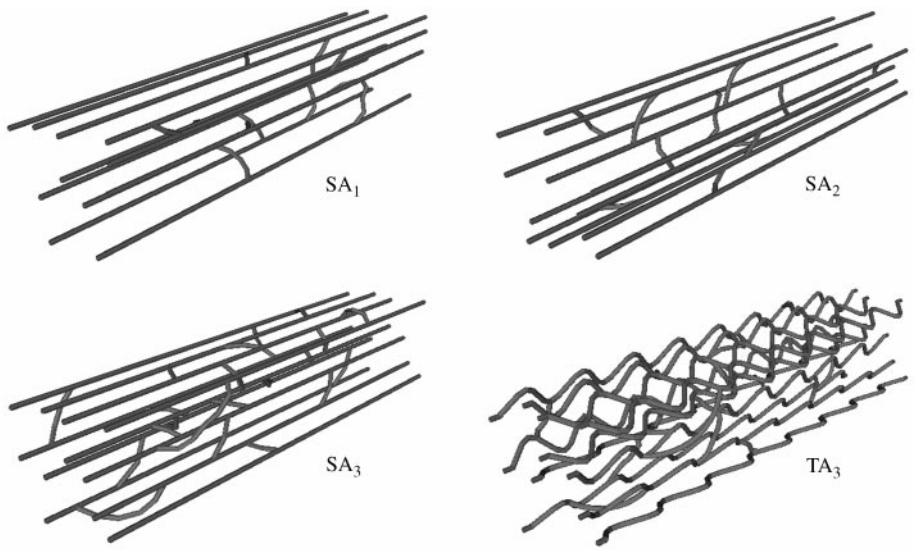

FIG. 2. Capillary networks SA_1, SA_2, SA_3, and TA_3, where the subscripts refer to the realization. Except for the random (R) networks, all networks with the same subscript are geometrically related. For example, SU_3, SA_3, TU_3, and SU_3-counter are based on the same parallel vessel arrangement as TA_3, but differ in the presence or absence of anastomoses, parallel vessel tortuosity, or countercurrent flow.

TABLE 2
*Results of blood flow simulations**

	Blood flow ($pl\ s^{-1}$)			Erythrocyte flow ($pl\ s^{-1}$)		
Geometry	Min	Mean	CV	Min	Mean	CV
SU	6.0	6.0	0	2.6	2.6	0
SA	0.8	5.5	0.30	0.1	2.3	0.29
TA	0.7	5.6	0.29	0.1	2.4	0.27

* Statistics shown are for all vessel segments in each network and are calculated using all realizations for each network type: SU, SA, and TA.

heterogeneity. However, the effect was small and was reversed when tortuosity was added (TA networks). The amount of flow heterogeneity found here is smaller than that observed experimentally when data from many capillary modules are pooled together (Klitzman & Johnson, 1982; Klitzman *et al*., 1983; Popel & Dawant, 1986; Duling & Damon, 1987; Ellsworth *et al*., 1988). A more relevant study is that of Ellis *et al*. (1994), who found as much as $\sim$47% spatial heterogeneity in the erythrocyte supply rate for modules supplied by a single arteriole in rat EDL muscle. The difference of $\sim$17% from the present results could be due to the branching structure from the arteriole which supplies capillaries in actual modules and the multiple, non-uniform venular outlets. Incorporating experimentally measured geometry of this type is an important next step in understanding flow-related transport heterogeneity.

Geometric Factors in Oxygen Transport

We investigated the oxygen-transport significance of four structural properties of capillary networks: (1) the constraint on the location of parallel capillaries due to the arrangement of muscle fibers; (2) the existence of tortuosity in parallel capillaries, especially in contracting striated muscle; (3) the existence of anastomotic cross-connections between parallel capillaries; (4) the existence of countercurrent flow in any group of "parallel" capillaries. An indication of the effects of these properties on oxygen transport can be seen in Fig. 4, which shows the spatial oxygen distributions obtained for cases SU_3, R_3, TA_3, and SU_3-counter.

A summary of our oxygen transport results is given in Table 3. Results for tissue oxygen delivery are shown graphically in Fig. 5, where oxygen transport statistics are shown relative to the reference case of muscle fiber-structured parallel

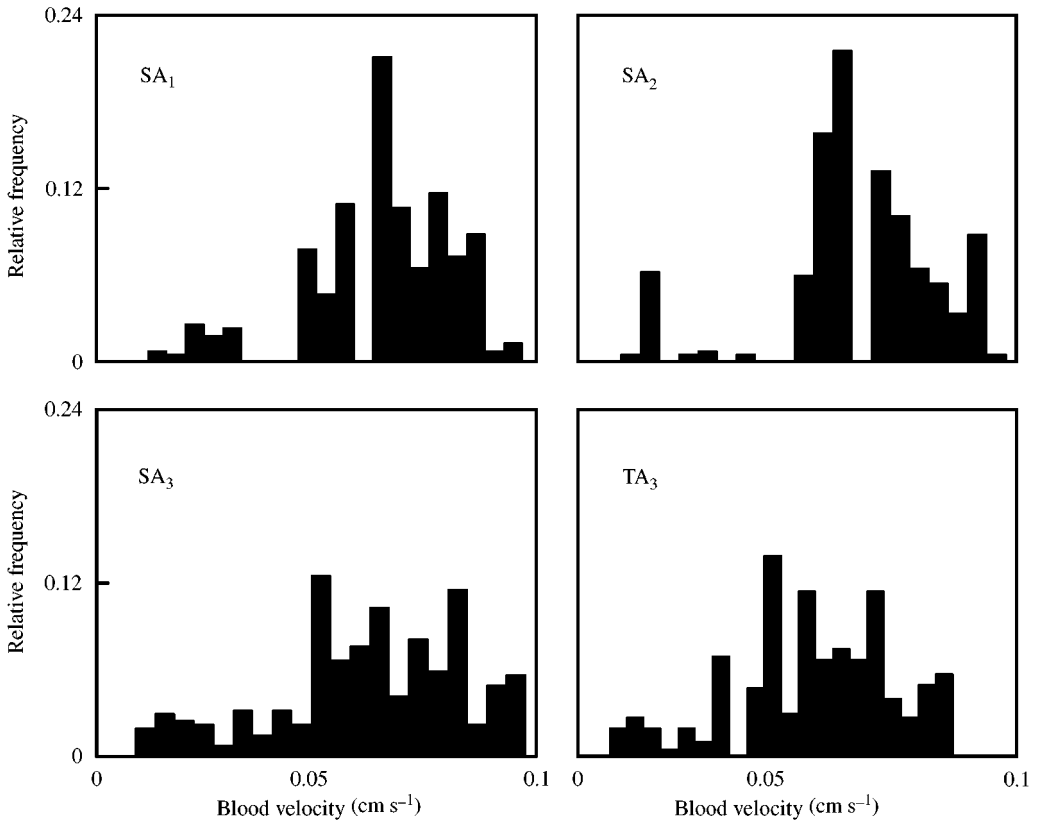

FIG. 3. Histograms of blood velocity distribution in networks SA_1, SA_2, SA_3, and TA_3.

capillaries (SU). The underlying muscle-fiber geometry, vessel tortuosity and anastomoses, and countercurrent flow were all found to be important determinants of the oxygen transport properties of capillary networks.

MUSCLE-FIBER GEOMETRY

The geometry of muscle fibers was seen to be of considerable importance in oxygen transport. In the absence of the muscle-fiber constraint (R networks), minimum tissue PO_2 decreased from 5.1 to 3.1 mmHg and the CV of tissue PO_2 increased from 0.28 to 0.33. Thus, oxygen transport heterogeneity and the likelihood of localized tissue hypoxia both increase when this underlying capillary/fiber structure is neglected. The muscle-fiber geometry is important because it produces a more uniform distribution of parallel capillaries (see below) and therefore more homogeneous transport characteristics. A comparison of the distribution functions for tissue PO_2 produced by the SU and R networks is shown in Fig. 6. The existence of larger regions of potential hypoxia in the R networks can be seen in the spatial oxygen distributions in Fig. 4.

To compare the heterogeneity of capillary spacing in the R and SU networks, we estimated sub-domain sizes using the closest-individual method (Kayar *et al.*, 1982). For each realization, we covered the 2D tissue cross-section (excluding a 5 μm border) with 10^4 uniformly spaced points and computed the distance to the nearest capillary, yielding a frequency distribution of domain sizes (radii). The domain size for the R networks was 12.0 ± 6.1 μm (mean $\pm$ S.D.), vs. 11.6 ± 5.5 μm for the SU case. Significantly, besides having lower means and being more narrow, the distributions for the SU networks had lower maximum sizes (29.1, 33.4, and 27.8 μm, respectively, for the three realizations, vs. 35.1, 35.9, and 35.6 μm for the R case). Thus, the larger heterogeneity in domain sizes produced by the R networks is the source of the observed increase in

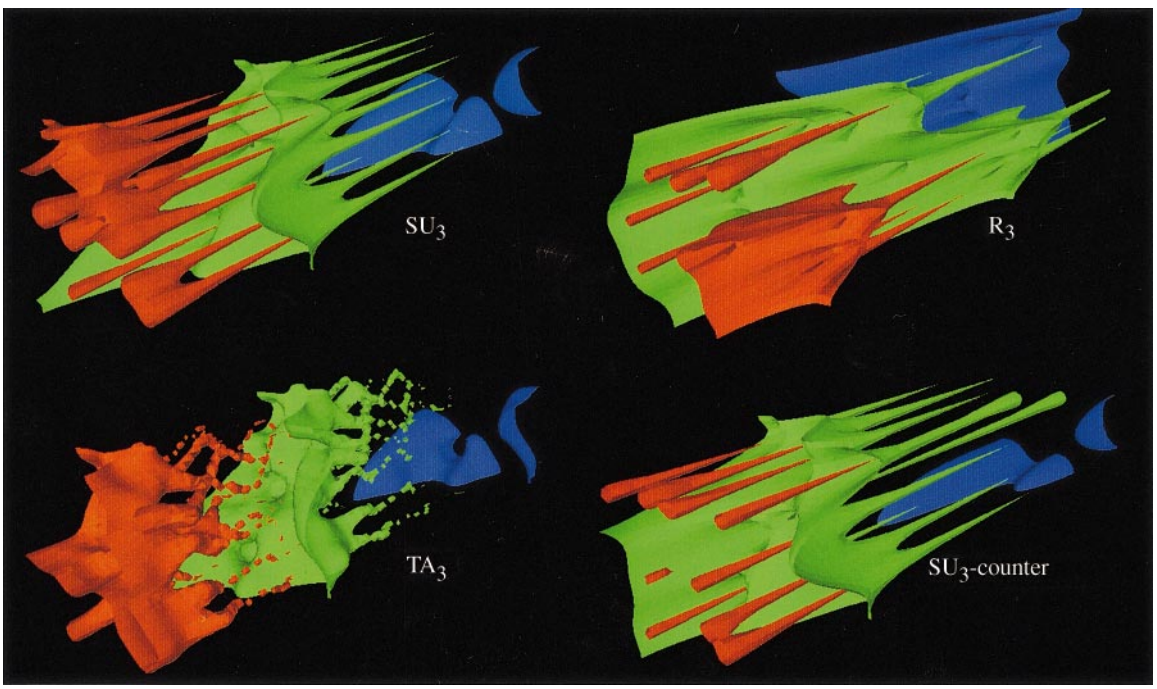

FIG. 4. Spatial oxygen distributions produced by various network types. The figure shows the same three isosurfaces of tissue PO_2 (30, 23, and 12 mmHg; red, green, and blue, respectively), for networks SU_3, R_3, TA_3, and SU_3-counter. The irregular pattern of isosurfaces seen for TA_3 occurs when the plotting routine attempts to follow the highly tortuous capillaries.

TABLE 3
*Results of oxygen transport simulations**

	Tissue PO_2 (mmHg)			End-capillary SO_2		
Geometry	Min	Mean	CV	Min	Mean	CV
SU	5.1	20	0.28	0.22	0.31	0.12
R	3.1	19	0.33	0.20	0.31	0.17
SU-counter	5.6	19	0.24	0.22	0.31	0.13
SA	5.0	20	0.29	0.23	0.29	0.13
TU	5.0	21	0.27	0.21	0.30	0.13
TA	5.5	21	0.27	0.22	0.29	0.13
TA_1-rest	25	31	0.10	0.45	0.46	0.013
TA_1	5.5	20	0.29	0.23	0.30	0.15

*Statistics are calculated using all realizations for each network type: SU (straight unbranched), R (random), SU-counter (straight unbranched countercurrent), SA (straight anastomosed), TU (tortuous unbranched), and TA (tortuous anastomosed). A single realization for resting muscle is also shown (TA_1-rest), along with the corresponding working case (TA_1).

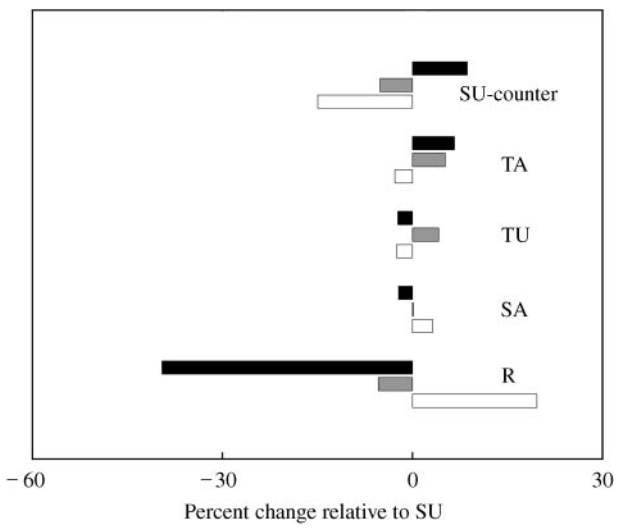

FIG. 5. Results for tissue oxygen delivery. The minimum, mean, and CV of tissue PO_2 for network types R, SA, TU, TA, and SU-counter are shown relative to the reference case SU. (■) min; (▒) mean; (□) CV.

oxygen transport heterogeneity. A similar result was obtained by Hoofd & Turek (1996), who found that capillaries distributed randomly in 2D produced much broader PO_2 histograms than uniformly spaced capillaries.

TORTUOSITY

Vessel tortuosity was found to significantly improve oxygen transport when combined with

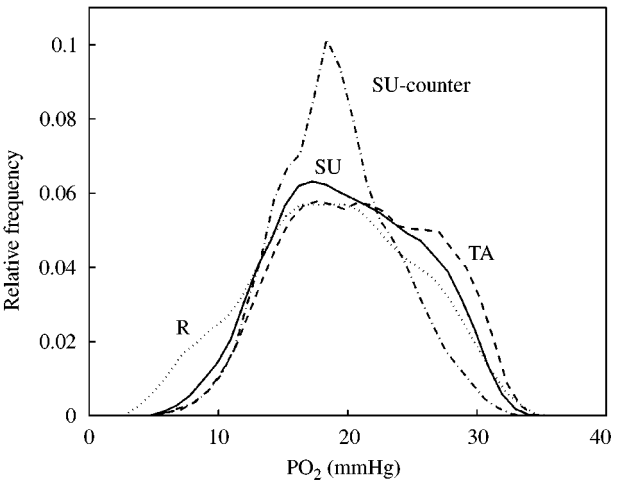

FIG. 6. Tissue PO_2 distribution functions for network types SU, R, TA, and SU-counter.

anastomoses. By itself, the addition of tortuosity (TU networks) increased mean tissue PO_2 by 5% and decreased CV(PO_2) slightly, but also decreased minimum PO_2. Therefore, transport heterogeneity decreased but the possibility of hypoxia increased, so the effect of tortuosity alone was ambiguous. In combination with anastomoses, however, the addition of tortuosity (TA networks) increased both minimum and mean tissue PO_2 by more than 5%, and decreased CV(PO_2). Thus, the combined effect was increased oxygen transport and decreased tissue oxygen heterogeneity.

Tortuosity changes the capillary network geometry and increases the surface area. The greater surface area and erythrocyte residence time in the networks with tortuosity allowed the extraction of more oxygen from the capillaries, as seen in the increased mean tissue PO_2. However, the PO_2 in the low-oxygen regions became slightly lower, suggesting that more oxygen was removed upstream. Combining anastomoses and tortuosity improved all transport characteristics, presumably due to favorable flow redistribution in addition to increased surface area and residence time. This improvement relative to the SU networks can be seen in the oxygen distribution function for the TA networks, shown in Fig. 6.

ANASTOMOSES

Anastomotic cross-connections, by themselves, did not significantly affect transport

characteristics. Mean tissue PO_2 remained almost unchanged in the SA networks, relative to the SU networks, minimum PO_2 decreased slightly, and $CV(PO_2)$ increased slightly. The observed increase in transport heterogeneity is somewhat surprising, since anastomoses might be expected to decrease blood flow heterogeneity and therefore produce more homogeneous oxygen distributions. The explanation for the present results is the exact uniformity of hematocrit and SO_2 inputs to the parallel vessels in our model, which cannot be expected in the physiological case. The fact that anastomoses were found to have only a small effect is due to the relatively small CVs of erythrocyte flux produced by the anastomoses.

The small effect of anastomoses observed here is consistent with the results of Popel *et al.* (1986), who found a significant increase in spatial heterogeneity [$CV(PO_2) = 0.58$ for contracting muscle, compared to a maximum of $CV(PO_2) = 0.3$ in the present study] only for relatively large CVs of erythrocyte flux and inlet PO_2 (0.6 and 0.2, respectively, compared to maximum values of 0.3 and 0 in the present study). As discussed above, our results for flow heterogeneity in a single capillary module are in the range of experimental values (0.3 vs. 0.47). The variation of inlet PO_2, taken here to be uniform, has not been measured for individual modules but is expected to be small. Without considering modules, Ellsworth *et al.* (1988) measured a CV of inlet capillary SO_2 of 0.14.

The oxygen-transport role of anastomoses given non-uniform inputs has not yet been investigated, but it seems that the amount of heterogeneity in tissue PO_2 distributions found experimentally (Klitzman *et al.*, 1983) and shown in numerical simulations to require large supply heterogeneity must have its origin above the level of the capillary module. Whether the necessary heterogeneity in capillary inlet SO_2 occurs at the terminal arterioles or at a higher level remains to be investigated.

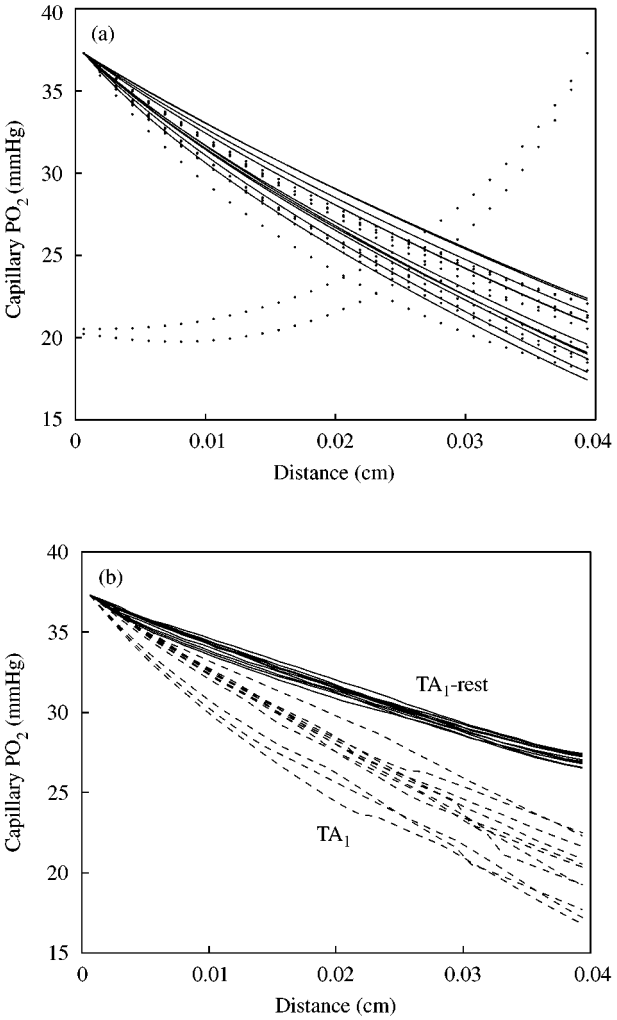

FIG. 7. Longitudinal variation of intracapillary oxygen content. PO_2 in the parallel vessel segments is shown as a function of z for (a) networks SU_2 and SU_2-counter; (——) SU_2; (·····) SU_2-counter, and (b) networks TA_1 and TA_1-rest. Sharp changes in PO_2 indicate the presence of anastomoses between parallel vessels.

COUNTERCURRENT FLOW

Figure 7(a) shows a typical pattern of intracapillary PO_2 for one of the countercurrent networks studied. Countercurrent flow was found to improve oxygen delivery, increasing minimum tissue PO_2 from 5.1 to 5.6 mmHg and decreasing $CV(PO_2)$ from 0.28 to 0.24 when 2 of 11 parallel capillaries were given countercurrent flows. As Fig. 4 shows, the presence of countercurrent flow significantly affects spatial oxygen distributions. This effect can also be seen in the PO_2 distribution function for the countercurrent networks, shown in Fig. 6. Thus, while the degree of countercurrent flow varies greatly between different tissues, its presence is seen to have important consequences and must be considered.

END-CAPILLARY SO_2

We have discussed the effect of four geometric factors on tissue oxygen distribution. These factors also affect capillary oxygen content, and additional understanding of oxygen delivery heterogeneity can be gained by examining SO_2 at the venous ends of the parallel capillaries (S_{ec}). These results are shown in Table 3. It can be seen that the absence of the muscle-fiber construction in the R networks greatly increases CV(S_{ec}) and decreases minimum S_{ec}, indicating a large increase in delivery heterogeneity. By contrast, all the network types based on the muscle-fiber geometry, including SU-counter, have nearly the same CV(S_{ec}). This is another indication of the importance of the underlying muscle-fiber geometry in determining oxygen transport characteristics of capillary networks. Note that mean S_{ec} varied slightly between cases with essentially the same consumption due to the fact that flow-weighted averages were not used.

RESTING MUSCLE

The increased importance of oxygen delivery heterogeneity in exercise can be seen by examining a case of resting muscle, TA_1-rest. As Table 3 shows, compared to the exercise case, TA_1, minimum and mean values of both tissue PO_2 and end-capillary SO_2 increased greatly, while CV(PO_2) and CV(S_{ec}) decreased by factors of 3 and 11, respectively. The relative homogeneity in the resting case, specifically the equilibration of capillary PO_2, can also be seen in longitudinal plots of intracapillary PO_2, shown in Fig. 7(b).

Vessel Blockages and Anastomoses

To examine one possible role of anastomoses, 2 of the 11 parallel vessels in the SU and SA networks were partially blocked. This was done by artificially increasing the resistance (by approximately a factor of 10) in several vessel segments of each SU network and removing the analogous segments in the SA networks, giving network types SU- and SA-blocked. The resulting blood flows were then calculated and used in oxygen transport simulations, after being corrected to maintain constant flow per unit tissue volume. In the SU networks the blockages decreased flow in two parallel vessels, while in the SA networks blockages caused flow to be redistributed to other parallel vessels, with flow possibly returning to a blocked parallel vessel downstream of the blocked segments. A similar study of flow in capillary networks with anastomoses was done by Hudetz (1993), who found that blockages in these networks produced a small increase in total flow resistance up to a critical blockage fraction of $\sim$30%. Beyond this "percolation limit" flow resistance increased very sharply, which would not happen for purely parallel capillaries and therefore indicates a possible drawback of capillary networks containing anastomoses.

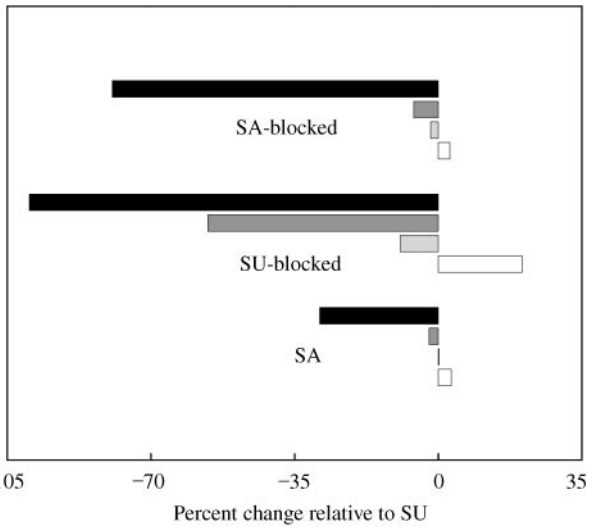

FIG. 8. Results for networks with blockages. The minimum of erythrocyte volume flux in parallel vessel segments and the minimum, mean, and CV of tissue PO_2 are shown for network types SA, SU-blocked, and SA-blocked relative to the SU networks. (■) min F; (■) min P; (□) mean P; (□) CV(P).

Our results for networks with blockages are given in Fig. 8. Both hemodynamic and oxygen transport consequences of vessel blockage were found to be large for the unbranched networks, and were greatly reduced by the presence of anastomoses. For the SU-blocked networks, minimum erythrocyte flux dropped from 2.6 to 0 pl s^{-1} and CV(F) rose from 0 to 0.47, and there was a corresponding decrease in minimum tissue PO_2 and increase in CV(PO_2). By comparison, the SA-blocked networks showed relatively small increases in hemodynamic and transport heterogeneity. These results demonstrate the

importance of anastomoses in maintaining oxygen delivery when parallel vessels become blocked, for example by white blood cells or due to vessel injury. This steady-state finding also applies to transient capillary blockages having time scales longer than a few seconds, which occur often under normal conditions.

Summary

Using our computational model, we have studied oxygen transport under physiological conditions and obtained results on the importance of several structural properties of capillary networks in striated muscle. We found that capillary tortuosity enhances oxygen transport. We also found that capillary anastomoses do not have a significant effect under normal conditions, but decrease transport heterogeneity when vessel blockages are present. In addition, we found that the network structure produced by muscle fibers is an important factor in oxygen transport and that countercurrent flow can greatly increase the efficiency of oxygen delivery.

The results presented here are for relatively small capillary networks, and do not include arterioles or venules. Thus, significant sources of oxygen delivery heterogeneity, including most of those due to flow effects, have been omitted. However, the results obtained indicate the role of several aspects of microvascular structure that have not been systematically investigated. To confirm and extend these results, studies of larger, more complete networks, including those obtained by three-dimensional reconstruction from *in vivo* experiments, are needed.

This work was supported by NIH grants HL-18292 and HL-09595.

REFERENCES

ALTMAN, P. L. & DITTMER, D. S. (1971). *Respiration and Circulation.* Bethesda: Fed. Am. Soc. Exp. Biol., p. 139.

BENNETT, R. A. O., PITTMAN, R. N. & SULLIVAN, S. M. (1991). Capillary spatial pattern and muscle fiber geometry in three hamster striated muscles. *Am. J. Physiol.* **260,** H579–H585.

BENTLEY, T. B., MENG, H. & PITTMAN, R. N. (1993). Temperature dependence of oxygen diffusion and consumption in mammalian striated muscle. *Am. J. Physiol.* **264,** H1825–H1830.

BERG, B. R. & SARELIUS, I. H. (1995). Functional capillary organization in striated muscle. *Am. J. Physiol.* **268,** H1215–1222.

CHRISTOFORIDES, C., LAASBERG, L. H. & HEDLEY-WHYTE, J. (1969). Effect of temperature on solubility of O_2 in human plasma. *J. Appl. Physiol.* **26,** 56–60.

CLARK Jr., A., FEDERSPIEL, W. J., CLARK, P. A. A. & COKELET, G. R. (1985). Oxygen delivery from red cells. *Biophys. J.* **47,** 171–181.

DONG, M. (1997). Influence of aging on oxygen transport in the microcirculation of skeletal muscle. Ph.D. Thesis, Virginia Commonwealth University.

DULING, B. R. & DAMON, D. H. (1987). An examination of the measurement of flow heterogeneity in striated muscle. *Circ. Res.* **60,** 1–13.

EGGLETON, C. D., ROY, T. K. & POPEL, A. S. (1998). Predictions of capillary oxygen transport in presence of fluorocarbon additives. *Am. J. Physiol.* **275,** H2250–H2257.

ELLIS, C. G., ELLSWORTH, M. L., PITTMAN, R. N. & BURGESS, W. L. (1992). Application of image analysis for evaluation of red blood cell dynamics in capillaries. *Microvasc. Res.* **44,** 214–225.

ELLIS, C. G., WRIGLEY, S. M. & GROOM, A. C. (1994). Heterogeneity of red blood cell perfusion in capillary networks supplied by a single arteriole in resting skeletal muscle. *Circ. Res.* **75,** 357–368.

ELLSWORTH, M. L., POPEL, A. S. & PITTMAN, R. N. (1988). Assessment and impact of heterogeneities of convective oxygen transport parameters in capillaries of striated muscle: experimental and theoretical. *Microvasc. Res.* **35,** 341–362.

ELLSWORTH, M. L. & PITTMAN, R. N. (1990). Arterioles supply oxygen to capillaries by diffusion as well as by convection. *Am. J. Physiol.* **258,** H1240–H1243.

ELLSWORTH, M. L., ELLIS, C. G., POPEL, A. S. & PITTMAN, R. N. (1994). Role of microvessels in oxygen supply to tissue. *News Physiol. Sci.* **9,** 119–123.

GROEBE, K. (1990). A versatile model of steady state O_2 supply to tissue. Application to skeletal muscle. *Biophys. J.* **57,** 485–498.

GROEBE, K. & THEWS, G. (1989). Effects of red cell spacing and red cell movement upon oxygen release under conditions of maximally working skeletal muscle. *Adv. Exp. Med. Biol.* **248,** 175–185.

HONIG, C. R. & GAYESKI, T. E. J. (1982). Correlation of O_2 transport on the micro and macro scale. *Int. J. Microcirc. Clin. Exp.* **1,** 367–380.

HOOFD, L. & TUREK, Z. (1996). Realistic modeling of capillary spacing in dog gracilis muscle greatly influences the heterogeneity of calculated tissue oxygen pressures. *Adv. Exp. Med. Biol.* **388,** 333–340.

HUDETZ, A. G. (1993). Percolation phenomenon: the effect of capillary network rarefaction. *Microvasc. Res.* **45,** 1–10.

JAPEE, S. A. (1999). A new video image analysis system to study red blood cell dynamics and oxygenation in capillary networks. Ph.D. Thesis, Virginia Commonwealth University.

JURGENS, K. D., PETERS, T. & GROS, G. (1994). Diffusivity of myoglobin in intact skeletal muscle cells. *Proc. Natl. Acad. Sci. U.S.A.* **91,** 3829–3833.

KAYAR, S. R., ARCHER, P. G., LECHNER, A. J. & BANCHERO, N. (1982). The closest-individual method in the analysis of the distribution of capillaries. *Microvasc. Res.* **24,** 326–341.

KIANI, M. F., PRIES, A. R., HSU, L. L., SARELIUS, I. H. & COKELET, G. R. (1994). Fluctuations in microvascular blood flow parameters caused by hemodynamic mechanisms. *Am. J. Physiol.* **266,** H1822–H1828.

KLITZMAN, B. & JOHNSON, P. C. (1982). Capillary network geometry and red cell distribution in hamster cremaster muscle. *Am. J. Physiol.* **24,** H211–H219.

KLITZMAN, B., POPEL, A. S. & DULING, B. R. (1983). Oxygen transport in resting and contracting hamster cremaster muscles: experimental and theoretical microvascular studies. *Microvasc. Res.* **25,** 108–131.

KROGH, A. (1919). The number and distribution of capillaries in muscles with calculations of the oxygen pressure head necessary for supplying the tissue. *J. Physiol.* (*London*) **52,** 409.

MAHLER, M., LOUY, C., HOMSHER, E. & PESKOFF, A. (1985). Reappraisal of diffusion, solubility, and consumption of oxygen in frog skeletal muscle, with applications to muscle energy balance. *J. Gen. Physiol.* **86,** 105–134.

MATHIEU-COSTELLO, O. (1987). Capillary tortuosity and degree of contraction or extension of skeletal muscles. *Microvasc. Res.* **3,** 98–117.

MATHIEU-COSTELLO, O., HOPPELER, H. & WEIBEL, E. R. (1989). Capillary tortuosity in skeletal muscles of mammals depends on muscle contraction. *J. Appl. Physiol.* **66,** 1436–1442.

MENG, H., BENTLEY, T. B. & PITTMAN, R. N. (1993). Myoglobin content of hamster striated muscles. *J. Appl. Physiol.* **74,** 2194–2197.

PAPADOPOULOS, S., ENDEWARD, V., JURGENS, K. D. & GROS, G. (2000). The diffusion coefficient of myoglobin in radial direction within living skeletal muscle fibers. *FASEB J.* **14,** A50.

PITTMAN, R. N. (1995). Influence of microvascular architecture on oxygen exchange in skeletal muscle. *Microcirculation* **2,** 1–18.

POPEL, A. S. (1989). Theory of oxygen transport to tissue. *Crit. Rev. Biomed. Eng.* **17,** 257–321.

POPEL, A. S. & DAWANT, B. (1986). Flow heterogeneity in microvascular networks: Comparison of theoretical predictions with experimental data. In: *Microvascular Networks*: *Experimental and Theoretical Studies* (Popel, A. S. & Johnson, P. C., eds), pp. 210–220. Basel: S. Karger.

POPEL, A. S., CHARNY, C. K. & DVINSKY, A. S. (1986). Effect of heterogeneous oxygen delivery on the oxygen distribution in skeletal muscle. *Math. Biosci.* **81,** 91–113.

PRIES, A. R., SECOMB, T. W., GAEHTGENS, P. & GROSS, J. F. (1990). Blood flow in microvascular networks: experiments and simulations. *Circ. Res.* **67,** 826–834.

PRIES, A. R., SECOMB, T. W., GESSNER, T., SPERANDIO, M. B., GROSS, J. F. & GAEHTGENS, P. (1994). Resistance to blood flow in microvessels in vivo. *Circ. Res.* **75,** 904–915.

ROY, T. K. & POPEL, A. S. (1996). Theoretical predictions of end-capillary PO_2 in muscles of athletic and non-athletic animals at VO_{2max}. *Am. J. Physiol.* **271,** H721–H737.

SECOMB, T. W. & HSU, R. (1994). Simulation of O_2 transport in skeletal muscle: diffusive exchange between arterioles and capillaries. *Am. J. Physiol.* **267,** H1214–H1221.

SULLIVAN, S. M. & PITTMAN, R. N. (1984). In vitro O_2 uptake and histochemical fiber type of resting hamster muscles. *J. Appl. Physiol.* **57,** 246–253.

WANG, D., KREUTZER, U., CHUNG, Y. & JUE, T. (1997). Myoglobin and hemoglobin rotational diffusion in the cell. *Biophys. J.* **73,** 2764–2770.

APPENDIX

Derivation of Intravascular Transport Equation

If we consider the plasma and erythrocyte spaces separately, we can write the following two steady-state convective transport equations:

$$\text{plasma} \qquad v_b(1 - H_D)\frac{\partial}{\partial \xi}(\alpha_{pl}P_{pl}) + \frac{1}{\pi R}\oint j\,\mathrm{d}\theta - \frac{1}{\pi R^2}J = 0, \tag{A.1}$$

$$\text{erythrocyte} \qquad v_b H_D \frac{\partial}{\partial \xi}(\alpha_{cell}P_{cell} + C_{Hb}S(P_{cell})) + \frac{1}{\pi R^2}J = 0, \tag{A.2}$$

where P_{pl}, P_{cell}, and S are volume-averaged plasma PO_2, erythrocyte PO_2, and erythrocyte SO_2, respectively. The parameters in the above two-compartment model are the blood velocity, v_b, the discharge hematocrit, H_D, the plasma and erythrocyte oxygen solubilities, α_{pl} and α_{cell}, the oxygen-binding capacity of hemoglobin, C_{Hb}, and the vessel radius, R. The capillary–tissue oxygen flux, j, is computed using the mass transfer coefficient k as shown in eqn (7). Note that calculations of k included a detailed description of $Hb–O_2$ kinetics inside the erythrocyte as well as O_2 transport in the plasma, as described previously (Popel, 1989; Eggleton *et al*., 1998). J is the erythrocyte–plasma oxygen flux per unit capillary length for an average PO_2 difference of $(P_{cell} - P_{pl})$. J will depend on the local hematocrit and can be expressed in terms of an erythrocyte–plasma mass transfer coefficient:

$$J = k_2(P_{cell} - P_{pl}). \tag{A.3}$$

To derive eqn (5), we add eqns (A.1) and (A.2). The J terms cancel, and letting $P_{pl} = P_{cell} = P_b$, we obtain

$$v_b H_D \frac{\partial}{\partial \xi}(\alpha_{cell}P_b + C_{Hb}S(P_b)) + v_b(1 - H_D)\frac{\partial}{\partial \xi}(\alpha_{pl}P_b) + \frac{1}{\pi R}\oint j\,\mathrm{d}\theta = 0. \tag{A.4}$$

If we now define α_b as in eqn (6) and let $P_b(S)$ be the inverse of the oxyhemogoblin dissociation function, we obtain

$$v_b \frac{\partial}{\partial \xi} (H_D C_{Hb} S + \alpha_b P_b(S)) + \frac{1}{\pi R} \oint j \, d\theta = 0. \tag{A.5}$$

Using the chain rule, the above derivative term becomes $v_b(H_D C_{Hb} + \alpha_b \, dP_b/dS) \partial S/\partial \xi$. Dividing eqn (A.5) by $(H_D C_{Hb} + \alpha_b \, dP_b/dS)$ then gives eqn (5) for intravascular oxygen transport. For the current case, where the oxygen-carrying capacity of plasma is relatively small, the approximation $P_{pl} = P_{cell}$ leads to minimal errors and allows plasma-dissolved oxygen to be included despite the absence of experimental or theoretical results for k_2. Alternatively, one could assume a small fixed difference $P_{pl} = P_{cell} - \Delta P$, in which case an equation identical to eqn (5) would be obtained but with $P_b = P_{cell} - (1 - H_T) \Delta P$.